Exp Brain Res (2015) 233:2695–2705
DOI 10.1007/s00221-015-4339-0

RESEARCH ARTICLE

Diagnosis of posttraumatic stress disorder (PTSD) based on correlations of prewhitened fMRI data: outcomes and areas involved

Peka Christova[1,2] · Lisa M. James[1,3] · Brian E. Engdahl[1,2,4] · Scott M. Lewis[1,5] · Apostolos P. Georgopoulos[1,2,3,5]

Received: 17 February 2015 / Accepted: 24 May 2015 / Published online: 13 June 2015

Abstract Successful diagnosis of PTSD has been achieved using neural correlations from prewhitened magnetoencephalographic (MEG) time series (Georgopoulos et al. in J Neural Eng 7:16011, 2010. doi:10.1088/1741-2560/7/1/016011; James et al. 2015). Here, we show that highly successful classification of PTSD and control subjects can be obtained using neural correlations from prewhitened resting-state fMRI data. All but one PTSD (14/15; sensitivity = 93.3 %) and all but one control (20/21; specificity = 95.2 %) subjects were correctly classified using 15 out of 2701 possible correlations between 74 brain areas. In contrast, correlations of the same but non-prewhitened data yielded chance-level classifications. We conclude that, if properly processed, fMRI has the prospect of aiding significantly in PTSD diagnosis. Twenty-five brain areas were most prominently involved in correct subject classification, including areas from all cortical lobes and the left pallidum.

Keywords PTSD · fMRI classification · Prewhitening · Biomarkers

✉ Apostolos P. Georgopoulos
omega@umn.edu

[1] Brain Sciences Center, Minneapolis Veterans Affairs Health Care System, Minneapolis, MN 55417, USA

[2] Department of Neuroscience, University of Minnesota Medical School, Minneapolis, MN 55455, USA

[3] Department of Psychiatry, University of Minnesota Medical School, Minneapolis, MN 55455, USA

[4] Department of Psychology, University of Minnesota Medical School, Minneapolis, MN 55455, USA

[5] Department of Neurology, University of Minnesota Medical School, Minneapolis, MN 55455, USA

Introduction

Posttraumatic stress disorder (PTSD) is a disabling condition, resulting from exposure to traumatic events. Symptoms include intrusive re-experiencing of the trauma, avoidance of trauma-related stimuli, and alterations in cognition, mood, arousal, and reactivity (American Psychiatric Association 2013). Approximately 7 % of the general population meets lifetime criteria for PTSD (Kessler et al. 2005), with much higher prevalence rates reported among certain subgroups such as military veterans (Hoge et al. 2004, 2006; Seal et al. 2007). Diagnosis of PTSD currently relies on self-reporting of symptoms; however, there has been increased interest in identifying objective biomarkers of PTSD to facilitate diagnosis.

To that end, a number of studies have utilized functional neuroimaging such as functional magnetic resonance imaging (fMRI) to evaluate neural abnormalities associated with PTSD. Indeed, various studies have implicated anomalies in several brain regions including the amygdala, medial prefrontal cortex, insula, hippocampus, and cingulate cortex (Etkin and Wager 2007; Lanius et al. 2006; Patel et al. 2012). However, method variance across studies has resulted in inconsistent findings regarding areas involved with PTSD as well as conflicting reports of hyperactivation in some studies and hypoactivation of the same areas in other studies. Furthermore, many studies investigating neural abnormalities associated with PTSD have used symptom provocation tasks (e.g., script-driven imagery), potentially confounding task-associated neural processes with those specific to PTSD. In order to better clarify neural mechanisms specifically associated with PTSD, researchers have recently turned to resting-state functional neuroimaging studies.

Resting-state neuroimaging permits characterization of intrinsic neural processes that complement those observed

in task-related research and facilitates comparison of brain activity between those affected with PTSD and controls. Similar to the task-related findings discussed above, resting-state fMRI studies of PTSD have identified neural abnormalities involving the insula, prefrontal cortex, cerebellum, and visual cortex (Yin et al. 2011) as well as the amygdala, cingulate cortex, and thalamus (Yan et al. 2013). In addition, several fMRI studies have demonstrated aberrant functional connectivity between seed regions such as the amygdala (Brown et al. 2014; Rabinak et al. 2011; Sripada et al. 2012) and cingulate cortex (Kennis et al. 2015; Lanius et al. 2010; Bluhm et al. 2009) with other areas. Although delineating the functional abnormalities associated with particular regions is worthwhile in terms of understanding the pathophysiology of PTSD, seed-based analyses are inherently constrained to specific regions of interest. Recent whole-brain functional connectivity analyses have demonstrated disruptions primarily between the frontal cortex and cortico-limbic circuit (Jin et al. 2014), consistent with prevailing neurocircuitry models of PTSD (Rauch et al. 2006; Liberzon and Garfkinkel 2009).

Identification of resting-state abnormalities associated with PTSD sets the groundwork for advancement beyond basic discovery of underlying pathophysiology toward clinical applications such as diagnostic classification. Two recent studies have utilized various features derived from resting-state fMRI (e.g., amplitude of low-frequency fluctuations [ALFF], temporal connectivity, spatial connectivity) to evaluate the ability to accurately classify individuals as PTSD or controls subsequent to surviving an earthquake (Li et al. 2014) or motor-vehicle accident (Liu et al. 2015). These studies demonstrated that ALFF alone discriminates individuals with PTSD from controls with 80 % accuracy (Li et al. 2014) and that performance improves as additional functional connectivity features (i.e., temporal, spatial) are included (Liu et al. 2015). With the inclusion of 500 features, classification accuracy was observed to be >90 %, with limbic and prefrontal areas providing the most discriminant features (Liu et al. 2015). These studies are highly promising in terms of the utility of fMRI in discriminating between individuals with PTSD and controls; however, additional research is warranted to further substantiate the utility of fMRI in classification of PTSD and to evaluate classification accuracy in other trauma-exposed populations.

Using MEG, we have previously identified anomalies in resting-state neural communication that distinguish individuals with and without PTSD with >90 % accuracy (Georgopoulos et al. 2010; James et al. 2015). Furthermore, we demonstrated that fewer than 40 predictors were sufficient to achieve highly accurate classification (Georgopoulos et al. 2010). Subsequent research suggested that neural anomalies in the right temporal and parieto-occipital areas distinguished PTSD from healthy controls (Engdahl et al. 2010; James et al. 2013). These studies provide compelling evidence of a PTSD biomarker based on neural communication derived from MEG. However, the clinical utility of MEG in regard to PTSD is hampered by the relative lack of availability of MEG scanners in comparison with fMRI, which is widely available. Therefore, in the present study, we apply a similar strategy to that used in our prior MEG research to evaluate classification accuracy in fMRI data obtained from veterans with PTSD and trauma-exposed veteran controls.

Materials and methods

Participants

Veterans participating in a larger study evaluating biomarkers of PTSD described in detail elsewhere (James et al. 2013) were invited to participate in the present study if they had either a primary diagnosis of PTSD or, for the control group, no lifetime history of PTSD symptoms and no current clinically significant mental health symptoms. Fifteen veterans with a primary diagnosis of PTSD (13 men) and 21 healthy control veterans (20 men) participated in the study. The age differed significantly between the control (62.7 $\pm$ 1.65 y, mean $\pm$ SEM, $N = 21$) and PTSD (48.8 $\pm$ 4.06 y, $N = 15$) groups ($P = 0.005$, independent samples t test, equal variances not assumed). All but two participants were Caucasians (one control participant was African American and one PTSD participant was Native American/African American). Those who agreed to participate completed diagnostic interviews including the Clinician-Administered PTSD scale (CAPS; Blake et al. 1995) and Structured Clinical Interview for DSM-IV-TR (SCID; First et al. 2002) to re-evaluate diagnostic status, and underwent an fMRI. The mean $\pm$ SEM CAPS scores were 1.33 $\pm$ 0.691 (control, $N = 21$) and 70.93 $\pm$ 2.345 (PTSD, $N = 15$) The study protocol was approved by the Institutional Review Board at the Minneapolis VA Medical Center, and subjects provided written informed consent prior to the study.

Data acquisition

All data were acquired using a 3T MR scanner (Achieva, Philips Healthcare, Best, The Netherlands) with an eight-channel phased-array SENSitivity Encoding (SENSE) (Pruessmann et al. 1999) SENSE-HEAD-8 head coil for reception. For each subject, a high-resolution T1-weighted anatomical image Turbo Field Echo (TFE) was obtained (168 sagittal slices, TR = 8.0928 ms, TE = 3.697 ms, voxel

size = 0.9375 × 0.9375 × 1 mm). fMRI was acquired using Fast Field Echo (FFE) transversal (axial) with whole-brain coverage (repetition time TR = 2000 ms, echo time TE = 30 ms, flip angle = 90 deg, 40 axial slices per volume with slice scanning order ascending, no interleaving, voxel size = 2.75 × 2.75 × 3.5 mm). One hundred and fifty consecutive whole-brain fMRI volumes were obtained for 14 subjects and 203 volumes for 22 subjects, corresponding to 6000 or 8120 images, respectively.

Image preprocessing

A 704-core high-performance Linux computer cluster (Rocks 5.4, CentOS 5.5) with MATLAB R2012 (64 bit), Analysis of Functional NeuroImages (AFNI), Surface Mapping (SUMA), and FreeSurfer (FS) 5.0.0 was used for data processing. All imaging data were analyzed using the AFNI software package (Cox 1996). The first 3 volumes of each BOLD time series were discarded to allow for equilibrium magnetization. All remaining volumes were slice-time corrected and registered to the volume of the time series collected nearest in time to the acquisition of the anatomical scan. Motion correction was done using a Python script. Alignment of anatomical to functional MRI was done using a Python script with cost function local Pearson's correlation (Saad et al. 2009). Individual brains were then registered to the stereotactic space of Talairach and Tournoux (1988) using a 12-parameter-affine registration. The transformation applied to the anatomical image was applied to the functional image together with resampling to the original voxel size. Cortical surface and subcortical brain areas, identified with FreeSurfer, were used as masks to extract the voxel time series. Data from 74 cortical and subcortical areas (37 in the left and 37 in the right hemisphere) were used, excluding the cerebellum (due to incomplete coverage), and medial orbital cortex and gyrus rectus (due to poor signal quality). The following areas were used: amygdala, angular gyrus, calcarine fissure, caudate, anterior cingulate, mid-cingulate, posterior cingulate, cuneus, inferior frontal gyrus (opercular), inferior frontal gyrus (orbital), inferior frontal gyrus (triangular), middle frontal gyrus, superior frontal gyrus, fusiform gyrus, heschl gyrus, hippocampus, insula, lingual gyrus, inferior occipital gyrus, middle occipital gyrus, superior occipital gyrus, pallidum, paracentral lobule, parahippocampal gyrus, inferior parietal gyrus, superior parietal gyrus, postcentral gyrus, precentral gyrus, precuneus, putamen, supramarginal gyrus, inferior temporal gyrus, middle temporal gyrus, middle temporal gyrus–temporal pole, superior temporal gyrus–temporal pole, superior temporal gyrus, and thalamus.

Data preprocessing

First, the coefficient of variation of the BOLD time series of each voxel was calculated, and voxel series with a coefficient of variation >5 % were eliminated from further analysis due to their likely proximity to large vessels (Kim et al. 1994). Next, single voxel BOLD time series were prewhitened using a Box-Jenkins (15,1,1) autoregressive integrated moving average (ARIMA) model (Box and Jenkins 1976), as described in detail in Christova et al. (2011). The resulting white noise innovations (residuals) were averaged across all the voxels within each area to obtain averaged time series of the innovations which were then used to calculate zero-lag cross-correlations between all possible pairs of areas ($N = 2701$ possible pairs of 74 areas). These zero-lag cross-correlations between i and j areas (CC_{ij}^0) were z-transformed (Fisher 1958) and were entered as potential predictors in the classification analysis below:

$$z_{ij}^0 = 0.5\ln\frac{\left(1 + CC_{ij}^0\right)}{\left(1 - CC_{ij}^0\right)}$$

Classification analyses

Method

We used the robust bootstrap-based method (Georgopoulos et al. 2010) to assess the classification potential of z_{ij}^0. This method taps on the variability in the z_{ij}^0 values (across subjects) by generating a large number of bootstrap samples (with different subject composition) and estimating probabilities for (intermediate) subject classifications using predictors independently of their classification outcome. A final decision on group assignment is then made based on the summed probabilities (over the bootstraps), with the higher probability for a specific group assignment deciding the winner. The procedure is explicated in detail in Georgopoulos et al. (2010) and is summarized in the schematic diagram of Fig. 1. In the present application, we performed 70,000 bootstraps using the following parameters (letters correspond to those in Georgopoulos et al. 2010): number of predictors, $K = 15$; bootstrap sample size for both groups, $B = 100$; measure for predictor selection, ξ = signal-to-noise ratio (SNR; item #4 in Appendix A in Georgopoulos et al. 2010); number of iterations for predictor selection, $M = 3$; number of preliminary intermediate group assignments, $L = 7$; number of final intermediate group assignments, $L' = 101$; and number of repetitions R' of $L' = 1000$. Classification outcomes were expressed as specificity, sensitivity, odds ratio, and receiver operating characteristic (ROC) curve. Sensitivity and specificity were defined as follows:

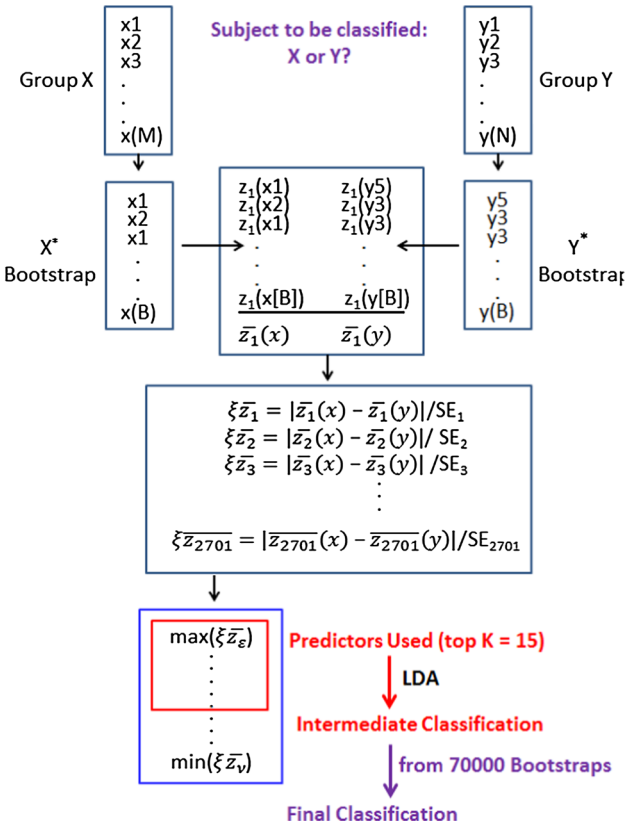

Fig. 1 Schematic diagram of the classification procedure employed, as follows (from *top* to *bottom*). **a** We are given a subject to be classified to one or the other of 2 groups, X and Y, of sample size M and N, respectively. **b** From the original X and Y groups, we generate two bootstrap samples with replacement, X* and Y*, of the same sample size B. **c** There are 2701 possible predictors for each subject (all possible pairwise zero-lag, z-transformed correlations between the 74 brain areas used). For each predictor, an average across all bootstrap sample subjects is calculated, and the absolute value of the difference between the two group averages computed. In addition, the standard error of the difference is also computed assuming unequal variances (see Eq. 4 in Appendix in Georgopoulos et al. 2010). The ratio of the absolute mean difference over its standard error is the signal-to-noise ratio (SNR) ξ ultimately used for selecting the predictors. **d** These ξ's are ranked and the top K = 15 are used as predictors in a linear discriminant analysis (LDA) where the unknown-group subject is classified using the subject's values of the same 15 predictors. LDA yields two probabilities of assignment, one for each group, which are retained for further use. This procedure is repeated for 70,000 bootstraps. **e** From this set of 70,000 bootstrap probabilities of group assignment, subsets of $L' = 101$ are chosen randomly, the respective group assignment probabilities are summed, and the result (subject assignment to X or Y group depending on the higher sum) is retained as an "intermediate" classification. Notice that this intermediate classification is "open loop" in the sense that its outcome does not influence subsequent steps of the procedure, i.e., the classification information is not back-propagated to shape future outcomes. **f** The latter procedure is repeated $R' = 1000$ times, and the subject is finally classified to the group with greater number of intermediate assignments. (More details of the procedure are given in Georgopoulos et al. 2010)

$$\text{Sensitivity} = \frac{\text{Number of PTSD patients correctly classified}}{\text{Total number of PTSD patients}}$$

$$\text{Specificity} = \frac{\text{Number of control participants correctly classified}}{\text{Total number of control participants}}$$

The following three measures of classification performance were calculated to summarize the results and test the null hypothesis that classification outcomes are due to chance. (a) Statistical significance was assessed using the Pearson Chi-square test, corrected for continuity (Snedecor and Cochran 1980) and Fisher's exact test. (b) 95 % confidence intervals for sensitivity and specificity were calculated using the conservative Wilson (1927) method. And (c) the standard error of the area under the curve (AUC) in the Receiver Operating Characteristic (ROC) analysis was calculated under the nonparametric assumption, and the asymptotic significance of the AUC was computed against the null hypothesis that AUC = 0.5. In addition, asymptotic 95 % confidence intervals were also computed. A computer program in FORTRAN was used for the classification analysis and generation of confidence intervals on the sensitivity and specificity values. Finally, the SPSS statistical package was used for general statistical testing (Chi-square, ROC curve, *t* tests, etc.).

Groups

Classification analyses were carried out for three different groups: each one composed of two member classes to which subjects were assigned based on specific criteria (actual disease diagnosis, randomly, and age median split). (a) Actual groups: This was the main goal of the study. The actual group assignment was used in 70,000 bootstraps. (b) Random group assignment: This analysis tested the hypothesis that classification performance in (a) above was not due to chance. For that purpose, the 36 subjects were assigned randomly to one of two groups and the classification outcomes compared to those obtained from the actual groups. One thousand bootstraps were used for this analysis. (c) Age effect: Since the age of subjects differed significantly between the two groups (see above), we carried out a separate analysis where two groups were constructed using a median split, irrespective of disease diagnosis. Two subjects had the same age (at the middle of the distribution), so they were assigned randomly to one or the other group. One thousand bootstraps were used for this analysis.

Non-prewhitened, filtered data

In this analysis, we assessed the classification power of non-prewhitened data. For that purpose, the voxel-wise raw

Table 1 Classification results using prewhitened data

	Predicted		Total
	PTSD	Control	
(a) Classification table			
Observed			
PTSD	14	1	15
Control	1	20	21
Total	15	21	36

Test	Value	DF	Significance (two sided)
(b) Analysis of the two-way classification table			
Pearson Chi-square (corrected for continuity)	24.7	1	$P = 0.0000001$
Fisher's exact test			$P = 0.00000001$

	Observed	95 % Confidence intervals	
		Lower bound	Upper bound
(c) Sensitivity, specificity, and Wilson (1927) confidence intervals			
Sensitivity	0.933	0.869	0.998
Specificity	0.952	0.906	0.999

AUC	SE	Significance	95 % Confidence intervals	
			Lower bound	Upper bound
(d) ROC analysis				
0.943	0.047	$P = 0.000008$	0.852	1.000

BOLD time series were filtered ($0.009 < f < 0.08$ Hz; Fox et al. 2005) and their z_{ij}^0 analyzed as above using 70,000 bootstraps.

Computation time

The major time consumption in the computations is due to the extensive bootstrapping. The 70,000 bootstraps of the present study would take approximately 24 h in a dual-processor quad-core personal computer; the prewhitening and correlations calculations would take approximately 18 h for the 36 subjects in this study. The computation time is substantially reduced by distributing the jobs to multiple nodes/processors in a computer cluster, as was in our case.

Results

Prewhitened data

Classification outcomes

The classification was excellent, with all but one subject in each group being correctly classified, namely 14/15 PTSD and 20/21 control (Table 1a). The probability values of both Chi-square and Fisher's exact tests were very highly significant (Table 1b). Both sensitivity and specificity were very high (Table 1c); sensitivity was 0.933 (93.3 %), specificity was 0.952 (95.2 %), and both of their respective lower bounds of the conservative (Wilson 1927) confidence intervals were well above 0.5, i.e., above the 50 % chance level. Finally, the AUC in the ROC analysis (Fig. 2, left panel) was very high and highly statistically significant (Table 1d), with a lower bound of its 95 % confidence interval (0.852) well above the chance level (AUC = 0.5) (Table 1d).

Group classification under random group assignment of prewhitened data

As expected, this resulted in very poor classification. The average sensitivity was 0.400 (0.273, 0.526; lower and upper bounds of Wilson 95 % confidence intervals) and the average specificity was 0.381 (0.207, 0.591).

Group classification under age median split assignment of prewhitened data

This also resulted in poor classification. The average sensitivity was 0.571 (0.365, 0.755; see above), and the average specificity was 0.533 (0.333, 0.781).

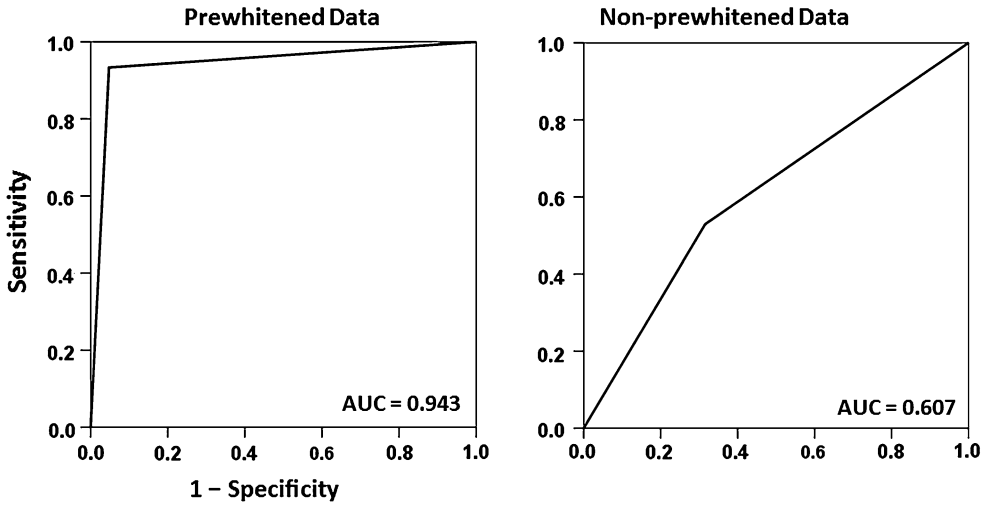

Fig. 2 ROC curves obtained using prewhitened and non-prewhitened data. Classification performance is excellent for the former and chance for the latter. AUC, area under the curve

Table 2 Classification results using non-prewhitened data

		Predicted		Total
		PTSD	Control	
(a) Classification table				
Observed				
PTSD		9	6	15
Control		8	13	21
Total		17	19	36
Test		Value	DF	Significance (two sided)
(b) Analysis of the two-way classification table				
Pearson Chi-square (corrected for continuity)		0.92	1	0.337
Fisher's exact test				0.311
		Observed	95 % Confidence intervals	
			Lower bound	Upper bound
(c) Sensitivity, specificity, and Wilson (1927) confidence intervals				
Sensitivity		0.600	0.374	0.815
Specificity		0.619	0.409	0.792
AUC	SE	Significance	95 % Confidence intervals	
			Lower bound	Upper bound
(d) ROC analysis				
0.607	0.096	$P = 0.274$	0.419	0.794

Classification outcomes for non-prewhitened, filtered data

Given that most resting fMRI studies in the literature use non-prewhitened, filtered data, we wanted to compare the outcome of the same analyses (as those described above for the original group classification using prewhitened data) on the same data without prewhitening but after filtering the BOLD time series, as is commonly done in resting-state fMRI studies. The classification was poor, as can be seen in Table 2. Figure 2 (right panel) shows the ROC curve, where the null hypothesis that the AUC does

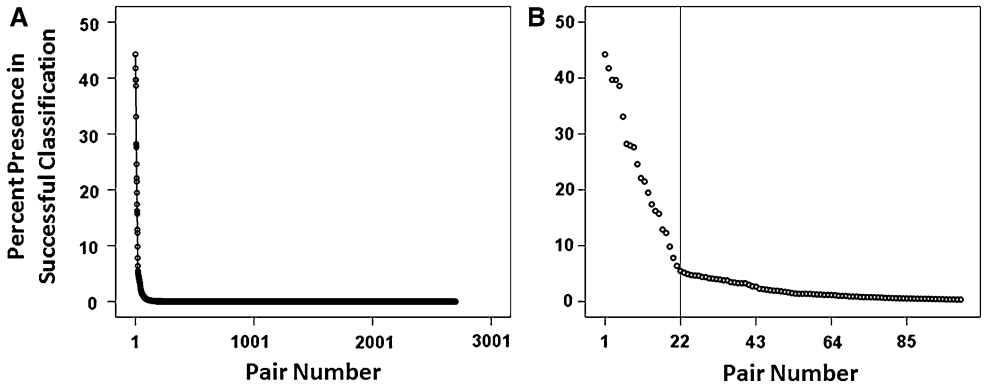

Fig. 3 The plots show how frequently a predictor (correlation between 2 areas) was present in a successful (for classification) predictor set. Predictors are rank ordered, depending on the frequency (percent) of their presence. **a** All pairs are shown; **b** only the first 100 pairs are shown. The *vertical line* is drawn at pair number 22 where an obvious break in the curve occurs. This means that the first 22 predictors were most frequently involved in correct group assignment

not differ from chance could not be rejected ($P = 0.274$, Table 2d).

Brain areas involved in correct subject classification using prewhitened data

As mentioned above, sets of 15 predictors were used in the classification analysis. Therefore, for any specific bootstrap sample, there were 15 predictors available, i.e., 15 correlations between pairs of areas. A given pair could only occur once in a set but a given area could have been represented more than once, depending on the number of pairs it could be part of. We sought to determine the relative weight/importance of the various pairs and associated areas for correct classification, as follows. In total, there were 36 subjects × 70,000 bootstraps = 2,520,000 bootstraps, and the probabilities for assigning a subject to one of the two groups formed the basis for the ultimate classification of the subject by summing a large number of these probabilities and deriving intermediate classifications, as illustrated in Fig. 1. However, to investigate the issue of the pairs and areas involved, we had to work at the level of a single bootstrap because this was the only level with a unique set of predictors. For that purpose, we analyzed the pair/area composition of 2,124,357 bootstrap samples which gave 100 % correct classification ("successful" predictor set) for a subject, as follows. First, we determined the frequency of the presence of each one of the 2701 pairs used in a successful predictor set. Figure 3a shows the plot of the ranked pairs. It can be seen that the vast majority of pairs had negligible presence, whereas a few pairs had a high presence. Figure 3b shows the plot of the 100 highest ranked pairs and shows a clear break in the curve at the 22nd rank (vertical line). Therefore, we analyzed in detail the area composition of those 22 pairs. Table 3 shows the areas for each one of these pairs, together with their frequency of occurrence in a successful set of 15 predictors. It can be seen that certain areas appeared several times in a successful set by being parts of several pairs. Therefore, the relative contribution of an area to successful classification stems from two components, namely (a) the rank of the pair containing the area (with rank #1 being the highest) and (b) the number of pairs in which the area appears. These two components can be combined to a single measure, overall rank, by summing the inverse of the ranks of all pairs in which the area appears. The results of this analysis are shown in Table 4. The following can be seen in Tables 3 and 4. (a) Altogether, 25 of the 74 areas used (33.8 %) contributed to successful classification sets. (b) The #1 pair was the correlation between right superior temporal pole and left pallidum (Table 3); interestingly, neither of those two areas appeared again in any other pair. (c) Left pallidum was the only subcortical area contained in the top 22 predictor pairs. And (d) both right and left hemispheric areas were involved from all major cortical lobes (frontal, parietal, occipital, and temporal).

Discussion

This study extends our previous approach in diagnosing PTSD using MEG (Georgopoulos et al. 2010; James et al. 2015) to fMRI. Although the sample size in the present study is small, the results obtained are excellent, attesting to the power of the method and its feasible application to fMRI data. For both MEG- and fMRI-based classification analyses, predictors were neural correlations calculated from prewhitened (i.e., stationary and non-autocorrelated) time series. Remarkably, as we show here, correlations calculated from the same data without prewhitening performed

Table 3 The highest ranked 22 predictor pairs

Rank	Frequency	Area 1 in the pair	Area 2 in the pair
1	44.2	Right superior temporal pole	Left pallidum
2	41.7	Right cuneus	Left middle occipital gyrus
3	39.7	Right angular gyrus	Right anterior cingulum
4	39.6	Left inferior frontal gyrus (opercular part)	Right superior temporal gyrus
5	38.6	Right angular gyrus	Left superior frontal gyrus
6	33.1	Left insula	Left middle temporal gyrus
7	28.2	Right hippocampus	Left insula
8	27.9	Left insula	Right superior temporal gyrus
9	27.6	Right angular gyrus	Left inferior frontal gyrus (orbital part)
10	24.6	Left inferior frontal gyrus (opercular part)	Left superior temporal gyrus
11	22.1	Right angular gyrus	Left anterior cingulum
12	21.5	Left cuneus	Left middle occipital gyrus
13	19.5	Right angular gyrus	Left hippocampus
14	17.4	Right angular gyrus	Left postcentral gyrus
15	16.2	Left hippocampus	Left insula
16	15.7	Left insula	Right middle temporal gyrus
17	12.9	Right postcentral gyrus	Left supramarginal gyrus
18	12.3	Right Heschl's gyrus	Right middle temporal gyrus
19	9.8	Right inferior frontal gyrus (orbital part)	Left insula
20	7.8	Right postcentral gyrus	Left middle temporal gyrus
21	6.4	Right inferior frontal gyrus (triangular part)	Right superior frontal gyrus
22	5.5	Right inferior frontal gyrus (triangular part)	Right superior temporal gyrus

Frequency denotes the percent of times a specific pair appeared within the 15-predictor successful classification set. The order of areas in a pair is arbitrary

poorly in classifying PTSD and control subjects. Therefore, rendering the time series stationary and non-autocorrelated is the key necessary and sufficient common requirement for successful classification for both MEG and fMRI data. Finally, as expected, random group assignment or median-age-split grouping resulted in poor classification.

In the present fMRI study, 15 predictors were adequate to yield excellent results. Since these came out of a total of 2701 possible predictors (all possible pairwise correlations between 74 areas), they represent 15/2701 = 0.55 % of the total. Similarly excellent results were obtained with 20 predictors (0.74 %). This then would be a good approximation of the minimum successful range (0.55–0.74 %). In our previous MEG study (Georgopoulos et al. 2010), sets of 30–40 predictors (out of 30,628) gave excellent results, which corresponds to a range of 0.10–0.13 %. Both fMRI and MEG intervals are very small and of comparable magnitude (<1 %). This indicates that powerful discriminant information is contained in remarkably small sets of neural correlations.

Our results provided interesting insights into the areas involved in correct classification. Out of 2701 possible pairwise correlations, only 22 (0.8 %) made a clear difference in that respect (Fig. 3b). The top ranked areas were the right superior temporal pole and left pallidum (Table 4). The former corresponds to the most intense spot identified in our previous MEG work (area marked A in Fig. 3 in Engdahl et al. 2010). The involvement of the pallidum could not have been discovered with MEG, given that pallidum is a subcortical structure and that MEG mainly detects cortical sources. It is interesting that the volume of the left pallidum was found to be reduced in survivors of a mine disaster (Chen et al. 2012). Although the exact role of the left pallidum in the pathophysiology of PTSD is not known, the involvement of the basal ganglia in this disorder can be attributed to their known connectivity with specific frontal areas. Although traditionally regarded as pure motor structures, detailed examination of their activity in behaving monkeys in the late 1970s revealed that cells in the dorsorostral part of the globus pallidus (Georgopoulos and DeLong 1978) and the rostromedial part of the subthalamic nucleus (DeLong and Georgopoulos 1978) were not movement related (DeLong and Georgopoulos 1979a, b; see DeLong and Georgopoulos 1981, for an extensive discussion). This observation led to the postulation in 1983 of non-overlapping cortico-basal ganglia loops (DeLong et al. 1983), namely a motor and a "complex" loop (see Fig. 1 in DeLong et al. 1983), a concept that was further documented, extended (DeLong et al. 1984a, b, 1985), and popularized later on (Alexander et al. 1986). The

Table 4 Areas contained in the 22 top predictor pair

Overall rank	Area	Pair rank	Sum of 1/pair rank
1.5	Right superior temporal pole	1	1
1.5	Left pallidum	1	1
3	Right angular gyrus	3, 5, 9, 11, 13, 14	0.884
4	Left insula	6, 7, 8, 14, 15, 16, 19	0.688
5	Left middle occipital gyrus	2, 12	0.583
6	Right cuneus	2	0.5
7	Right superior temporal gyrus	4, 8, 22	0.420
8	Left inferior frontal gyrus (Opercular part)	4, 10	0.35
9	Right anterior cingulum	3	0.333
10	Left middle temporal gyrus	6, 20	0.217
11	Left superior frontal gyrus	5	0.2
12	Left hippocampus	13, 15	0.144
13	Right hippocampus	7	0.143
14	Right middle temporal gyrus	16, 18	0.118
15.5	Left anterior cingulum	9	0.111
15.5	Left inferior frontal gyrus (orbital part)	9	0.111
17	Left superior temporal gyrus	10	0.1
18	Right inferior frontal gyrus (triangular part)	21, 22	0.093
19	Left cuneus	12	0.083
20.5	Right postcentral gyrus	17	0.059
20.5	Left supramarginal gyrus	17	0.059
22	Right Heschl's gyrus	18	0.056
23	Right inferior frontal gyrus (orbital part)	19	0.053
24	Left postcentral gyrus	20	0.05
25	Right superior frontal gyrus	21	0.048

Ranks with decimals indicate ties. The numbers in the 'pair rank' column refer to the rank of the pair in Table 3. The numbers in the 'sum of 1/pair rank' are the sums of the inverse of the numbers in the 'pair rank' column and reflect a weighted impact of a given area on the successful classification sets. The ordering of tied areas is arbitrary

pallidum receives topographically organized input from the striatum, such that rostral striatum projects to rostral pallidum (Hedreen and DeLong 1991), and the head of the caudate projects to the dorsal pallidum (Hazrati and Parent 1992). Thus, the "complex" part of the pallidum, namely its dorsorostral part (Georgopoulos and DeLong 1978; DeLong et al. 1983), receives projections from the caudate nucleus. Now, Van Hoesen et al. (1981) described widespread projections from various areas of the temporal lobe of the monkey to the head of the caudate nucleus. In addition, prefrontal areas interconnected to temporal ones were found also to share projections in the caudate nucleus (Yeterian and van Hoesen 1978). These findings document the existence of an extensive temporal/prefrontal cortex/orbitofrontal/inferior parietal lobule → caudate → rostrodorsal pallidum network and link the pallidal "complex" part to interconnected cortical association areas (Yeterian and van Hoesen 1978). Since the temporal pole shared with pallidum, the #1 rank presence in successful classification sets (Table 4), it is noteworthy that projections specifically from the temporal pole were directed almost exclusively to the head of the caudate nucleus (Van Hoesen et al. 1981). This provides an anatomical connectivity basis for the interactions observed in the present study. However, the lateralization of this temporal pole—pallidum interaction is puzzling: why the correlation between *right* temporal pole and *left* pallidum? The fact that this interaction is so prominent in differentiating control from PTSD brain patterns suggests that it is, indeed, unexpected and, therefore, may point to a PTSD-related abnormal communication. Given that interhemispheric homotopic areas are typically strongly interacting (Christova et al. 2011) and anatomically interconnected (Hedreen and Yin 1981), we propose that the correlated activity between right temporal pole and left pallidum could be accounted for by the following route: right temporal pole ↔ left temporal pole → left pallidum. This idea needs to be further investigated.

The third ranked area was the right angular gyrus (Table 4). This was the second most prominent approximate area identified with MEG (area marked B in Fig. 3

in Engdahl et al. 2010). There was also a broad correspondence between this fMRI and the previous MEG (Engdahl et al. 2010) studies with respect to right and left occipital and temporal areas involved. Some frontal and temporal areas identified with fMRI (e.g., inferior frontal opercular and orbital parts, hippocampus) would have been difficult to discern with MEG due to their deep location. Finally, a surprising finding was the absence of the amygdala, a structure associated with PTSD, from the top 22 pairs. Given the known involvement of the amygdala with fear mechanisms, a possible explanation of this finding would be that fear was low or absent during our resting-state fMRI acquisition, hence the lack of involvement of the amygdala. In addition, it should be noted that the predictors in our study are correlations between areas and not activation of an area itself. It is possible that the amygdala (and maybe other areas, see Etkin and Wager 2007; Lanius et al. 2006; Patel et al. 2012) was activated themselves, but their correlations with other areas did not make significant contributions to correct classification. Finally, it should be noted that other areas may be involved, e.g., areas we did not use for technical reasons (e.g., cerebellum, parts of orbital cortex; see "Materials and methods"). However, the set of 74 areas we used did provide subsets with excellent classification power.

These results open the prospect for using fMRI, a practically ubiquitous technology, to aid in PTSD diagnosis. The fact that our findings were obtained by employing (a) extensive bootstraps and (b) without supervised learning means that the results are very robust and that they may well generalize to larger samples. This hinges on the assumption that our actual samples of control and PTSD subjects are representative of their respective groups, which we believe they are. However, definite confirmation will have to await a large-scale clinical trial.

Finally, it should be noted that the current study used only cross-correlations between areas for the classification analyses, on the assumption that PTSD reflects fundamentally a miscommunication among specific brain areas. It is possible that other approaches might also prove useful in discriminating control and PTSD brain patterns, as exemplified, e.g., by recent studies that used combinations of more involved structural and/or functional analyses for that purpose (Li et al. 2014; Liu et al. 2015), with promising results (e.g., 80 % accuracy, Li et al. 2014). We believe that our approach is simpler (using just pairwise correlations) and better (>90 % sensitivity and specificity). However, these excellent results hinge on correlating stationary and non-autocorrelated (i.e., prewhitened) time series.

Acknowledgments This study was supported by a Service Directed grant from the US Department of Veterans Affairs, the University of Minnesota American Legion Brain Sciences Chair (A.P.G.), and the University of Minnesota Anderson Chair for PTSD Research (B.E.).

References

Alexander GE, DeLong MR, Strick PL (1986) Parallel organization of functionally segregated circuits linking basal ganglia and cortex. Annu Rev Neurosci 9:357–381

American Psychiatric Association (2013) Diagnostic and statistical manual for mental disorders, 5th edn. Author, Washington, DC

Blake DD, Weathers FW, Nagy LM, Kaloupek DG, Gusman FD, Charney DS, Keane TM (1995) The development of a clinician-administered PTSD scale. J Trauma Stress 8:75–90

Bluhm RL, Williamson PC, Osuch EA, Frewen PA, Stevens TK, Boksman K, Neufeld RW, Theberge J, Lanius RA (2009) Alterations in default network connectivity in posttraumatic stress disorder related to early-life trauma. J Psychiat Neurosci 34:187–194

Box GEP, Jenkins GM (1976) Time series analysis: forecasting and control. Holden-Day, San Francisco, CA

Brown VM, LaBar KS, Haswell CC, Gold AL, Beall SK, Van Voorhees E et al (2014) Altered resting-state functional connectivity of basolateral and centromedial amygdala complexes in posttraumatic stress disorder. Neuropsychopharmacology 39:361–369

Chen Y, Fu K, Feng C, Tang L, Zhang J, Huan Y, Cui J, Mu Y, Qi S, Xiong L, Ma C, Wang H, Tan Q, Yin H (2012) Different regional gray matter loss in recent onset PTSD and non PTSD after a single prolonged trauma exposure. PLoS ONE 7:e48298. doi:10.1371/journal.pone.0048298

Christova P, Lewis SM, Jerde TA, Lynch JK, Georgopoulos AP (2011) True associations between resting fMRI time series based on innovations. J Neural Eng 8:046025. doi:10.1088/1741-2560/8/4/046025

Cox RW (1996) AFNI: software for analysis and visualization of functional magnetic resonance neuroimages. Comput Biomed Res 29:162–173

DeLong MR, Georgopoulos AP (1978) The subthalamic nucleus and the substantia nigra of the monkey: neuronal activity in relation to movement. Soc Neurosci Abstr 4:42

DeLong MR, Georgopoulos AP (1979a) Physiology of the basal ganglia: a brief overview. Adv Neurol 23:137–153

DeLong MR, Georgopoulos AP (1979b) Motor functions of the basal ganglia as revealed by studies of single cell activity in the behaving primate. Adv Neurol 24:131–140

DeLong MR, Georgopoulos AP (1981) Motor functions of the basal ganglia. In: Handbook of physiology, the nervous system, brooks VB (volume editor), Brookhart JM, Mountcastle VB (section editors), Section 1, Volume II, Part 2. American Physiological Society, Bethesda, Maryland, pp 1071–1061

DeLong MR, Georgopoulos AP, Crutcher MD (1983) Cortico-basal ganglia loops. Exp Brain Res Suppl 7:30–40

DeLong MR, Alexander GE, Georgopoulos AP, Crutcher MD, Mitchell SJ, Richardson RT (1984a) Role of basal ganglia in limb movements. Human Neurobiol 2:235–244

DeLong MR, Georgopoulos AP, Crutcher MD, Mitchell SJ, Richardson RT, Alexander GE (1984b) Functional organization of the basal ganglia: contributions of single-cell recording studies. In: Functions of the basal ganglia, CIBA Foundation Symposium No. 107, pp 64–82

DeLong MR, Crutcher MD, Georgopoulos AP (1985) Primate globus pallidus and subthalamic nucleus: functional organization. J Neurophysiol 53:530–543

Engdahl B, Leuthold AC, Tan H-RM, Lewis SM, Winskowski AM, Dikel TN, Georgopoulos AP (2010) Post-traumatic stress disorder: a right temporal lobe syndrome? J Neural Eng 7:066005

Etkin A, Wager TD (2007) Functional neuroimaging of anxiety: a meta-analysis of emotional processing in PTSD, social anxiety disorder, and specific phobia. Am J Psychiatry 64:1476–1488

First MB, Spitzer RL, Gibbon M, Williams JBW (2002) Structured clinical interview for DSM-IV-TR axis I disorders, research version, non-patient edition (SCID-I/NP). Biometrics Research, New York State Psychiatric Institute, New York

Fisher RA (1958) Statistical methods for research workers, 13th edn. Oliver and Boyd, Edinburgh

Fox MD, Snyder AZ, Vincent JL, Corbetta M, Van Essen DC, Raichle ME (2005) The human brain is intrinsically organized into dynamic, anticorrelated functional networks. Proc Natl Acad Sci USA 102:9673–9678

Georgopoulos AP, DeLong MR (1978) The globus pallidus of the monkey: neuronal activity in relation to movement. Soc Neurosci Abstr 4:43

Georgopoulos AP, Tan H-M, Lewis SM, Leuthold AC, Winskowski AM, Lynch JK, Engdahl B (2010) The synchronous neural interactions test as a functional neuromarker for post-traumatic stress disorder (PTSD): a robust classification method based on the bootstrap. J Neural Eng 7:16011. doi:10.1088/1741-2560/7/1/016011

Hazrati LN, Parent A (1992) The striatopallidal projection displays a high degree of anatomical specificity in the primate. Brain Res 592:213–227

Hedreen JC, DeLong MR (1991) Organization of striatopallidal, striatonigral, and nigrostriatal projections in the macaque. J Comp Neurol 304:569–595. doi:10.1002/cne.903040406

Hedreen JC, Yin TC (1981) Homotopic and heterotopic callosal afferents of caudal inferior parietal lobule in Macaca mulatta. J Comp Neurol 197:605–621

Hoge CW, Castro CA, Messer SC, McGurk D, Cotting DI, Koffman RL (2004) Combat duty in Iraq and Afghanistan, mental health problems, and barriers to care. N Engl J Med 351:13–22

Hoge CW, Auchterlonie JL, Milliken CS (2006) Mental health problems, use of mental health services, and attrition from military service after returning from deployment to Iraq or Afghanistan. JAMA 295:1023–1032

James LM, Engdahl BE, Leuthold AC, Lewis SM, Van Kampen E, Georgopoulos AP (2013) Neural network modulation by trauma as a marker of resilience: differences between veterans with posttraumatic stress disorder and resilient controls. JAMA Psychiatry 70:410–418

James LM, Belitskaya-Lévy I, Lu Y, Wang H, Engdahl BE, Leuthold AC, Georgopoulos AP (2015) Development and application of a diagnostic algorithm for posttraumatic stress disorder. Psychiatry Res 231:1–7

Jin C, Qi R, Yin Y, Hu X, Duan L, Xu Q et al (2014) Abnormalities in whole-brain functional connectivity observed in treatment-naive post-traumatic stress disorder patients following an earthquake. Psychol Med 44:1927–1936

Kennis M, Rademaker AR, van Rooij SJ, Kahn RS, Geuze E (2015) Resting state functional connectivity of the anterior cingulate cortex in veterans with and without post-traumatic stress disorder. Hum Brain Mapp 36:99–109

Kessler RC, Berglund P, Demler O, Jin R, Merikangas KR, Walters EE (2005) Lifetime prevalence and age-of-onset distributions of DSM-IV disorders in the national comorbidity survey replication. Arch Gen Psychiatry 62:593–602

Kim SG, Hendrich K, Hu X, Merkle H, Ugurbil K (1994) Potential pitfalls of functional MRI using conventional gradient-recalled echo techniques. NMR Biomed 7:69–74

Lanius RA, Bluhm R, Lanius U, Pain C (2006) A review of neuroimaging studies in PTSD: heterogeneity of response to symptom provocation. J Psychiatr Res 40:709–729

Lanius RA, Bluhm RL, Coupland NJ, Hegadoren KM, Rowe B, Theberge J, Neufeld RW, Williamson PC, Brimson M (2010) Default mode network connectivity as a predictor of post-traumatic stress disorder symptom severity in acutely traumatized subjects. Acta Psychiatr Scand 121:33–40

Li X, Zhu D, Jiang X, Jin C, Zhang X, Guo L et al (2014) Dynamic functional connectomics signatures for characterization and differentiation of PTSD patients. Hum Brain Mapp 35:1761–1778

Liberzon I, Garfkinkel SN (2009) Functional neuroimaging in posttraumatic stress disorder. In: Shiromani PJ et al (eds) Posttraumatic stress disorder: basic science and clinical practice. Humana Press, New York, pp 297–317

Liu F, Xie B, Wang Y, Guo W, Fouche JP, Long Z et al (2015) Characterization of post-traumatic stress disorder using resting-state fMRI with a multi-level parametric classification approach. Brain Topogr 28:221–237. doi:10.1007/s10548-014-0386-2

Patel R, Spreng RN, Shin LM, Girard TA (2012) Neurocircuitry models of posttraumatic stress disorder and beyond: a meta-analysis of functional neuroimaging studies. Neurosci Biobehav Rev 36:2130–2142

Pruessmann KP, Weiger M, Scheidegger MB, Boesiger P (1999) SENSE: sensitivity encoding for fast MRI. Magn Reson Med 42:952–962

Rabinak CA, Angstadt M, Welsh RC, Kenndy AE, Lyubkin M, Martis B, Phan KL (2011) Altered amygdala resting-state functional connectivity in post-traumatic stress disorder. Front Psychiatry 2:62. doi:10.3389/fpsyt.2011.00062

Rauch SL, Shin LM, Phelps EA (2006) Neurocircuitry models of posttraumatic stress disorder and extinction: human neuroimaging research—past, present, and future. Biol Psychiat 60:376–382

Saad ZS, Glen DR, Chen G, Beauchamp MS, Desai R, Cox RW (2009) A new method for improving functional-to-structural MRI alignment using local Pearson correlation. Neuroimage 44:839–848

Seal KH, Bertenthal D, Miner CR, Sen S, Marmar C (2007) Bringing the war back home: mental health disorders among 103,788 US veterans returning from Iraq and Afghanistan seen at Department of Veterans Affairs facilities. Arch Intern Med 167:476–482

Snedecor GW, Cochran WG (1980) Statistical methods, 7th edn. Iowa State University Press, Iowa

Sripada RK, King AP, Garfinkel SN, Wang X, Sripada CS, Welsh RC, Liberzon I (2012) Altered resting-state amygdala functional connectivity in men with posttraumatic stress disorder. J Psychiatry Neurosci 37:241–249

Talairach J, Tournoux P (1988) Co-planar stereotaxic atlas of the human brain. Thieme, New York, NY

Van Hoesen GW, Yeterian EH, Lavizzo-Mourey R (1981) Widespread corticostriate projections from temporal cortex of the rhesus monkey. J Comp Neurol 199:205–219. doi:10.1002/cne.901990205

Wilson EB (1927) Probable inference, the law of succession, and statistical inference. J Am Stat Assoc 22:209–212

Yan X, Brown AD, Lazar M, Cressman VL, Henn-Haase C, Neylan TC et al (2013) Spontaneous brain activity in combat related PTSD. Neurosci Lett 547:1–5

Yeterian EH, Van Hoesen GW (1978) Cortico-striate projections in the rhesus monkey: the organization of certain cortico-caudate connections. Brain Res 139:43–63

Yin Y, Li L, Jin C, Hu X, Duan L, Eyler LT et al (2011) Abnormal baseline brain activity in posttraumatic stress disorder: a resting-state functional magnetic resonance imaging study. Neurosci Lett 498:185–189